IEEE Access
Multidisciplinary | Rapid Review | Open Access Journal

Received December 18, 2020, accepted January 8, 2021, date of publication January 11, 2021, date of current version January 20, 2021.

Digital Object Identifier 10.1109/ACCESS.2021.3050796

Research on Control Strategy of Two Dimensional Output Force Vibration Damping Electric Actuator

ZHENYANG HAO, TAO WANG, XIN CAO, (Member, IEEE), XUE LI, AND QIYAO ZHANG, (Student Member, IEEE)
Department of Electrical Engineering, Nanjing University of Aeronautics and Astronautics, Nanjing 210016, China
Corresponding author: Zhenyang Hao (zhenyang_hao@nuaa.edu.cn)

ABSTRACT The main spiral blades of helicopter and other non fixed wing aircraft are in the asymmetric and unsteady aerodynamic environment for a long time, which will make the body produce large-scale multi-directional low-frequency vibration, which will become the main vibration source of the body. The linear actuator can only produce single direction driving force, which is difficult to meet the high-precision vibration reduction requirements. Based on this, a direct drive vibration control system based on the space-time coupling method of rotating coordinate system is proposed. Firstly, the mathematical model of the output force of the single side of the electric actuator is deduced, and the space-time coupling method of the rotating coordinate system is proposed to derive the mathematical expression of the two-dimensional vibration suppression output force. Secondly, the two-dimensional output force control strategy based on the cross coupling control of multiple motors is proposed. The controller parameters are designed by state space method and the method of characteristic value of the feedback matrix to ensure the stability of the control system. The controller parameters are optimized according to the sensitivity H_∞ control theory to improve the anti-interference of the closed-loop system. Finally, a 14kg prototype is designed by the proposed control strategy, which completes the synchronous verification experiment of position and speed, steady state and dynamic verification experiment of output force. The experimental results show that the coordinated control strategy of multi motors proposed in this paper makes the actuator output force meet the performance requirements of the system vibration reduction and has a good stability.

INDEX TERMS Rotating frame space-time coupling method, cross-coupling control, state space method, hysteresis matrix eigen-value method, sensitivity H_∞ control.

I. INTRODUCTION

Helicopters are widely equipped in the military of various countries due to their strong mobility and assault. Compared with the fixed wing aircraft, helicopters have rotors and are exposed to harsh excitation environments for a long time, so there is a vibration problem that does not exist in the fixed wing aircraft, which brings safety hazards to the pilots' driving, and even causes aircraft damage and human death in serious cases [1], [2]. Therefore, how to improve or even eliminate the impact of body vibration on pilots and airborne equipment has become a research hotspot for research institutions and scientific researchers in universities around the world.

At present, the mainstream vibration reduction method is represented by the electric vibration damping actuator, and the linear force actuator is a typical electric vibration damping actuator [3], [4]. It drives a pair of meshing gears by controlling two servo motors, and drives two eccentric wheels to rotate in opposite directions at the same speed to output a single vibration absorbing force with a controllable amplitude and a single direction. The control structure is simple, but the mechanical structure is relatively complex. Therefore, researchers at home and abroad have carried out extensive research on linear force actuator.

Reference [5] points out that Pusan university of Korea has developed an electric vibration damper with adjustable output force and amplitude, which can adjust the force amplitude by changing the rotation radius of the eccentric wheel [5]. In the 1990s, the American scholar Kenneth D. Garnjost proposed in the reference [6] the use of a centrifugal electric vibration damping actuator structure, and dual servo motors to drive the eccentric load separately, and proposed a bilateral independent control mode algorithm with controllable output

The associate editor coordinating the review of this manuscript and approving it for publication was Ton Duc Do.

force and amplitude. In reference [3], a linear vibration damping actuator for active vibration reduction is proposed, and the joint simulation of FEM and MATLAB / Simulink is carried out, and the vibration elimination performance of the actuator is verified by experiments [3]. In reference [7], it is pointed out that the phase tracking control algorithm of adjustable mechanical active vibration absorber proposed by Lu Xiqun research group of Harbin Engineering University can realize on-line phase adjustment [3]. Reference [8] points out that the control strategy and control algorithm of on-line force actuator in Nanjing University of Aeronautics and Astronautics have been studied, and an experimental prototype has been developed, which has achieved a good vibration elimination effect [8].

However, with the increasing requirements for helicopter flight height, flight time and flight environment, higher requirements are put forward for the vibration reduction level of the body [9]. Because the linear force actuator can only output single direction power, it can not meet the increasing demand of vibration elimination. At the same time, the airborne equipment requires modularization, dexterous installation and convenient maintenance. Based on this, this paper presents a two-dimensional output force damping electric actuator, which can output 360 ° circular surface force, breaking the limitation of linear force actuator in outputting single direction force.

This paper is devoted to the system level theoretical analysis of single actuator. Firstly, the mathematical model of single side output force of vibration damping electric actuator is derived, and the space-time coupling method in rotating coordinate system is proposed. Based on this, the mathematical expression of two-dimensional output damping force of vibration damping electric actuator is derived [10]. Due to the coupling of the two-dimensional output damping force in time and space, this paper proposes a multi motor cross coupling control strategy. Through the state space method and the return matrix eigenvalue method, the parameters of each loop of the control system are designed, and the potential law of the external loop parameters of the control system and the stability of the system are theoretically clarified The sensitivity H_∞ control theory optimizes the controller parameters and improves the anti-interference performance of the closed-loop system. Finally, based on the designed 14kg experimental prototype, the performance verification experiment is completed, which provides theoretical and technical support for the later installation of the machine.

II. MODELLING AND CONTROL OF TWO-DIMENSIONAL OUTPUT FORCE

The structure diagram of the two-dimensional output force anti vibration electric actuator is shown in Figure 1. The four eccentric wheels are separately controlled by four motors, in which the transmission gear set is omitted, thus eliminating the influence of gear clearance nonlinearity on the control accuracy and making the control more flexible. Among the four eccentric wheels, the two eccentric wheels on the same side turn in the opposite direction, such as 1# and 2#, 3# and 4# eccentric wheels in Figure 2; and the two eccentric wheels in the same axis turn the same, such as 1# and 4#, 2# and 3# shown in Figure 2. According to the vibration force collected by the vibration sensor, four motors are controlled to make the frequency, amplitude and direction of the resultant force of the actuator output the same as the vibration force, and the phase is opposite to the vibration force, so that the active vibration reduction can be realized. In order to establish the two-dimensional output force mathematical model of the vibration damping actuator, the mathematical model of the unilateral output force of the actuator is first derived.

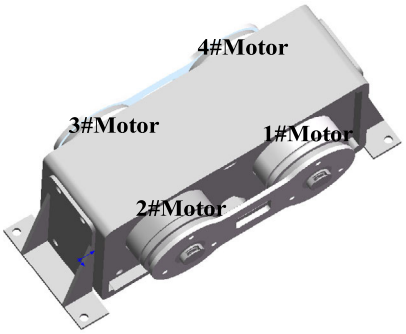

FIGURE 1. Two-dimensional output force vibration damping electric actuator structure diagram.

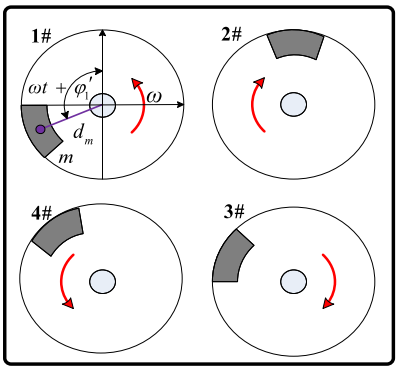

FIGURE 2. Working principle diagram of two-dimensional output force vibration damping electric actuator.

A. MODELLING OF UNILATERAL OUTPUT FORCE OF VIBRATION DAMPING ELECTRIC ACTUATOR

Taking the eccentric wheel side of 1# and 2# as an example, the force analysis is shown in Figure 3. 1# and 2# eccentric wheels are rotated in opposite direction, and the rotation

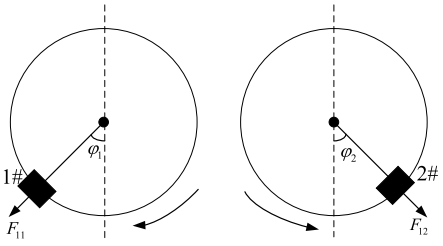

FIGURE 3. Force analysis diagram of unilateral eccentric wheel.

direction is shown in Figure 3. If eccentric wheel is regarded as a particle for force analysis, and air resistance and friction are ignored, centrifugal force on eccentric wheel is shown in formula (1) and (2):

$$F_{11} = m\omega^2 r\angle\varphi_1 \tag{1}$$
$$F_{12} = m\omega^2 r\angle\varphi_2 \tag{2}$$

Among them, F_{11} and F_{12} represent the centrifugal force on the 1# and 2# eccentric, m is the mass of the eccentric, and r is the distance from the eccentric particle to the center of rotation, φ_1 and φ_2 represent the position of 1# and 2# eccentric wheel.

By decomposing F_{11} and F_{12} into horizontal and vertical directions respectively, and defining horizontal right and vertical downward as positive directions, the horizontal and vertical components of actuator unilateral output force can be deduced as follows:

$$F_{1x} = 2m\omega^2 r\cos\left(\frac{\varphi_1+\varphi_2}{2}\right)\sin\left(\frac{\varphi_1-\varphi_2}{2}\right) \tag{3}$$
$$F_{1y} = 2m\omega^2 r\cos\left(\frac{\varphi_1+\varphi_2}{2}\right)\cos\left(\frac{\varphi_1-\varphi_2}{2}\right) \tag{4}$$

where F_{1x} and F_{1y} represent the horizontal and vertical components of the unilateral output force respectively. Then the output force of 1# and 2# eccentric side is as follows:

$$F_1 = 2m\omega^2 r\cos\left(\frac{\varphi_1+\varphi_2}{2}\right)\angle\left(\frac{\varphi_1-\varphi_2}{2}\right) \tag{5}$$

Similarly, the output force of 3# and 4# eccentric wheel side is as follows:

$$F_2 = 2m\omega^2 r\cos\left(\frac{\varphi_4+\varphi_3}{2}\right)\angle\left(\frac{\varphi_4-\varphi_3}{2}\right) \tag{6}$$

B. MODELLING OF TWO-DIMENSIONAL OUTPUT DAMPING FORCE BASED ON SPACE-TIME COUPLING METHOD IN ROTATING COORDINATE SYSTEM

If we want the vibration damping actuator to generate a actuation force F^* with an amplitude of F^*_{m} and a direction of φ^*, F^* can be decomposed into a horizontal component F^*_x and a vertical component F^*_y. It can be seen from Section II A that the unilateral component force generated by this actuator structure mentioned in this paper is a sinusoidal force with adjustable direction, adjustable phase and fixed force amplitude, but the amplitude of F^*_x is not always equal to that of F^*_y, so this method is no longer applicable. Therefore, based on the space-time coupling method of rotating coordinate system, the idea of orientation first and then force amplitude control is adopted in this paper, that is, the force components F_1 and F_2 on both sides of the actuator are controlled in the φ^* direction, and then the force amplitude is controlled by the coordinated control of the phases of F_1 and F_2, so as to realize the output of the given actuation force.

The space-time coupling method of rotating coordinate system can realize the orientation of output force.

To illustrate how to achieve the orientation of the output force, take 1# eccentric wheel and 2# eccentric wheel on the same side of the vibration damping actuator as an example. When the four motors of the actuator are started at the same time and reach a given speed, the positions of the 1# eccentric wheel and the 2# eccentric wheel are respectively φ_1 and φ_2 at the previous moment, and the direction of the unilateral actuation force F_1 is the negative direction of the y axis. At this time, if it is necessary to generate actuation force F_1', and F_1' rotates clockwise by δ angle compared with F_1. Rotate the x-y coordinate system clockwise by an angle of δ to obtain the x'-y' coordinate system. At this time, F_1', φ_1' and φ_2' in the $\mathrm{x}'-\mathrm{y}'$ coordinate system are equivalent to F_1, φ_1, and φ_2 in the x-y coordinate system. Among them, φ_1' and φ_2' are the current positions of 1# eccentric wheel and 2# eccentric wheel.

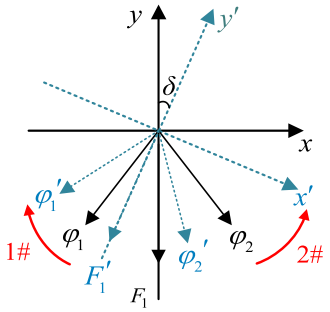

FIGURE 4. Direction diagram of eccentric wheel output force in rotating coordinate system.

Define 1# eccentric wheel clockwise rotation direction as positive direction, 2# eccentric wheel counterclockwise rotation direction as positive direction, we can get:

$$\varphi_1' = \varphi_1 + \delta$$
$$\varphi_2' = \varphi_2 - \delta \tag{7}$$

Since the amplitude of the centrifugal force received by the two eccentric wheels is equal, and the direction of the resultant output force F_1 is the negative direction of the y axis, $\varphi_1 = \varphi_2$. In order to make F_1' in the direction shown in Figure 4, the following conditions need to be met:

$$\frac{\varphi_1' - \varphi_2'}{2} = \delta \tag{8}$$

In the same way, the force direction of 3# and 4# eccentric wheels should be consistent with the force direction of 1# and 2# eccentric wheels, namely:

$$\frac{\varphi_4' - \varphi_3'}{2} = \delta \tag{9}$$

In the above formula, $\varphi'3$ and $\varphi'4$ are the phases of the 3# and 4# eccentric wheels in the $\mathrm{x}'-\mathrm{y}'$ coordinate system. Based on the space-time coupling method of rotating coordinate system, the resultant output force of the actuator can be adjusted to any direction of the two-dimensional plane. The contour of the output force is a circular surface, and the

radius of the circle is $2F_1$. At this time, F_1 and F_2 are in phase, as shown in Figure 5.

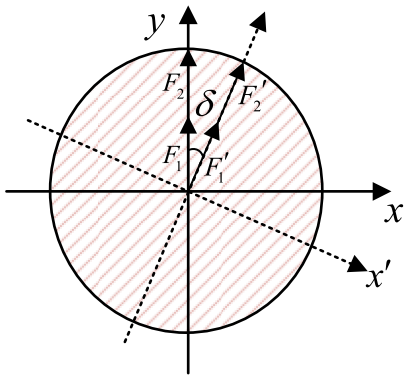

FIGURE 5. Output force contour diagram in rotating coordinate system.

Based on the space-time coupling method of the rotating coordinate system, first orient the unilateral force components of the vibration damping electric actuator to the same direction, that is:

$$\frac{\varphi_1 - \varphi_2}{2} = \frac{\varphi_4 - \varphi_3}{2} \tag{10}$$

On the basis of the same direction of output force on both sides of the actuator, combining equations (5) and (6) can realize the superposition of the component forces on both sides of the actuator in the same direction:

$$F = 4m\omega^2 r \cos\left(\frac{\varphi_1 - \varphi_4}{2}\right) \cos\left(\frac{\varphi_1 + \varphi_2 + \varphi_3 + \varphi_4}{4}\right) \angle\left(\frac{\varphi_1 - \varphi_2}{2}\right) \tag{11}$$

Among them, $\varphi_1 - \varphi_4 = (\varphi_1 + \varphi_2 - \varphi_3 - \varphi_4)/2$. Because:

$$\begin{cases} \varphi_1 = \omega t + \phi_1 \\ \varphi_2 = \omega t + \phi_2 \\ \varphi_3 = \omega t + \phi_3 \\ \varphi_4 = \omega t + \phi_4 \end{cases} \tag{12}$$

where $\phi_1, \phi_2, \phi_3, \phi_4$ are the initial positions of the eccentric wheels 1#, 2#, 3#, and 4# respectively. Therefore, formula (12) can be rewritten as:

$$F = 4m\omega^2 r \, cos\left(\frac{\varphi_1 - \varphi_4}{2}\right) \times cos\left(\omega t + \frac{\phi_1 + \phi_2 + \phi_3 + \phi_4}{4}\right) \angle\left(\frac{\varphi_1 - \varphi_2}{2}\right) \tag{13}$$

It can be seen from equation (13) that the frequency of the output force of the damping actuator is determined by the rotation speed of the four eccentric wheels. The amplitude of the output force is controlled by controlling the phase difference between the two coaxial eccentric wheels $\varphi_1 - \varphi_4$, and the direction of the output force is controlled by controlling the phase difference between the two eccentric wheels $\varphi_1 - \varphi_2$ on the same side. Changing the current phase of the four eccentric wheels can realize the change of the output force phase. However, the above formula derivation is based on the same speed of the four eccentric wheels. If there is a speed difference, the final output force of the actuator will appear beat frequency phenomenon [11]. Because the two-dimensional output force damping actuator omits the gear transmission mechanism, the motor load is large, and the eccentric load causes the motor speed fluctuation, which has adverse effects on the synchronous control of the eccentric wheel. How to maintain the strict synchronization of the rotation speed of the four eccentric wheels under the condition of outputting two-dimensional damping forces of different directions, different force amplitudes and different phases has become a difficulty for control. In addition, the control accuracy of the output force amplitude and direction is directly related to the control error of the position difference of the two eccentric wheels on the same side and coaxial. Therefore, the control core of the two-dimensional output force vibration damping actuator is the synchronous control of the rotation speed and position difference of the four eccentric wheels. Independent control realizes tracking control of output force by individually controlling each eccentric, but this method does not consider the coupling effect between the four motors. When one motor is disturbed, the other three motors will not react, so the anti-interference and synchronization are poor. Based on this, this paper proposes a multi-motor cross-coupling coordinated control strategy based on the space-time coupling method of the rotating coordinate system for the two-dimensional output force vibration damping actuator.

III. PARAMETER DESIGN AND OPTIMIZATION OF ELECTRIC ACTUATOR CONTROLLER

A. ANALYSIS OF MULTI-MOTOR CROSS-COUPLING CONTROL STRATEGY

Figure 6 indicates a block diagram of a two-dimensional output force control strategy based on multi-motor cross-coupling control. It should be noted that ACR and ASR are current loop regulators and speed loop regulators respectively. Among them, APR1 and APR4 represent the position difference loop regulators that control the power direction of the output on both sides, and APR3 is the position difference loop regulator that controls the amplitude of the output force, APR2 is a position average loop regulator that controls the phase of the output force.

To obtain the operating force with frequency ω^*, phase φ^*, direction θ^*, and amplitude F_a^*, according to equation (13), first obtain the actuator position difference on the same side set value $\Delta\varphi_1^*$, $\Delta\varphi_4^*$, coaxial position difference setting value $\Delta\varphi_3^*$ and phase setting value φ_2^* as follows:

$$\begin{cases} \Delta\varphi_1^* = \theta^* \\ \varphi_2^* = \omega^* t + \varphi^* \\ \Delta\varphi_3^* = \cos^{-1}\dfrac{F_a*}{4dm\omega^{*2}} \\ \Delta\varphi_4^* = \theta^* \end{cases} \tag{14}$$

The position average value of the four eccentric wheels is used as the feedback signal of the position average loop,

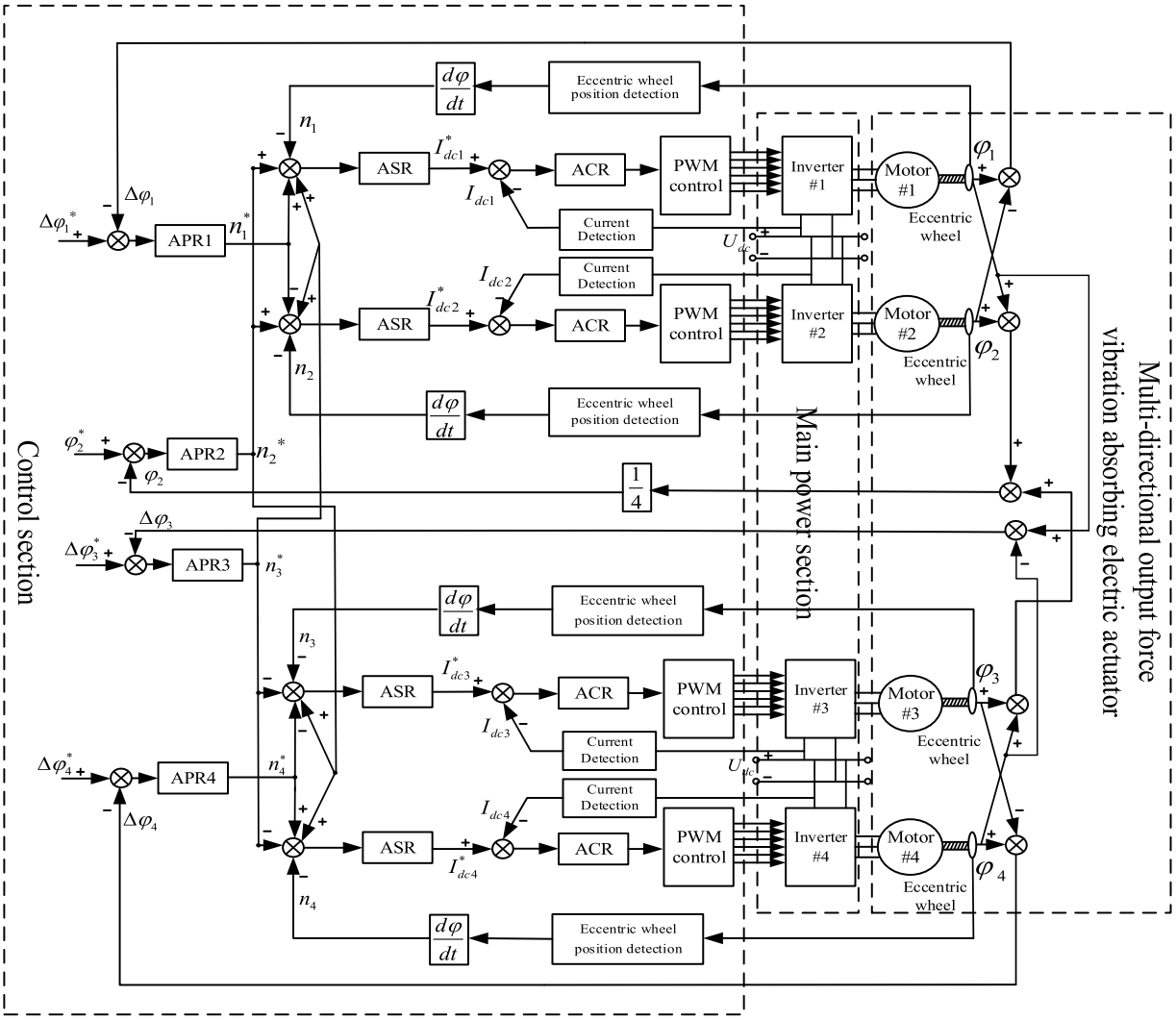

FIGURE 6. Block diagram of two-dimensional output force control strategy based on multi motor cross coupling control.

the difference between the feedback signal and the given position signal will be sent to APR2 for calculation. The achieved given speed signal will be transmitted to the four motors at the same time, enabling the synchronous control of the speed. The feedback signals of APR1 and APR2 are half of the position difference of 1# and 2# eccentric wheels and half of the position difference of 4# and 3# eccentric wheels on the same side. The value obtained by subtracting the feedback signal and the given signal will pass through the position difference loop regulator in the control direction. The relative speed signal will be positive for 1# and 4# motors, and negative for 2# and 3# motors. If the relative speed signal is positive, that is, the given signal is larger than the actual feedback signal, the 1# and 4# motors will accelerate while the 2# and 3# motors decelerate, so that the position difference of the two eccentric wheels on the same side is quickly widened until it reaches the given value. The position average loop is given as a periodic sawtooth wave whose frequency is consistent with the expected output force frequency.

Since the two-dimensional output force vibration damping actuator system is essentially a multiple-input multiple-output system, the traditional three-loop controller parameter design method is no longer applicable. Current loop and speed loop regulator, which belong to the inner loop of the motor, will adopt PI control to meet the loop demands of high frequency response. The method in literature [12] can be devoted to its parameter design. The position loop regulator employs proportional control, the emphases of above design are: Firstly, based on the stability margin, the hysteresis matrix eigenvalue method can determine the parameter stability region that satisfies the system phase angle margin and amplitude margin. Secondly, considering that the system load in this article is an eccentric load, the motor speed pulsation is large, which will affect the output force control accuracy, so it is necessary to introduce the load torque T_L into the control loop to establish a closed loop transfer function matrix from the disturbance T_L to the control error. Finally, combining the sensitivity H_∞ control theory, optimizing in the parameter stability domain to

TABLE 1. Motor parameters.

Parameters	Values
Rated voltage /V	28
Stator winding phase resistance R_m /Ω	0.28
Stator winding phase inductance L_m/mH	0.369
Torque constant K_T /(mNm/A)	136
Speed constant K_n /(rpm/V)	70.2
Mechanical time constant T_m/ms	7.66
Rotor equivalent moment of inertia J_m/g·cm^2	5060

improve the anti-interference performance of the closed-loop system.

B. CONTROLLER PARAMETER DESIGN

The specific parameters of the motor are shown in Table 1.

According to the loop parameter tuning method in the literature [12], the parameter results are listed in the following table:

TABLE 2. Controller inner loop parameters.

Parameters	Proportional coefficient	Integral coefficient
Current loop	0.47	751.6
Rotate speed loop	1.94	554.3

The closed-loop transfer function of the rotate speed loop can be equivalent to the first-order inertia link when designing the position loop parameters due to the settling time of the rotate speed loop is much faster than that of the position loop [13]:

$$\phi_n(s) = \frac{\omega_{cn}}{s + \omega_{cn}} \tag{15}$$

where ω_{cn} is the open-loop cutoff frequency of the rotate speed loop with the value 796rad/s. Since the control system mentioned in this article is a multiple-input multiple-output system, the open-loop transfer function in classical control theory is no longer applicable, so the open-loop transfer function matrix of the control system is derived by the state space method [14]. The state space is a mathematical description of the control system, usually composed of two mathematical equations, namely the state equation and the output equation, as shown in the following formula:

$$\dot{\boldsymbol{x}} = \boldsymbol{A}x + \boldsymbol{B}u \tag{16}$$

$$\boldsymbol{y} = \boldsymbol{C}x + \boldsymbol{D}u \tag{17}$$

Among them, $\boldsymbol{x}$ is the state vector in the system, $\dot{\boldsymbol{x}}$ represents the differential of the state vector, $\boldsymbol{\mu}$ and $\boldsymbol{y}$ represent the input vector and output vector in the system respectively. $\boldsymbol{A}$, $\boldsymbol{B}$, $\boldsymbol{C}$ and $\boldsymbol{D}$ are the matrices that express the relationship between the variables in the system, which are state matrix, input matrix, output matrix and feedforward matrix. In particular, when there is feedback in the control system, there is also a feedback matrix $\boldsymbol{H}$.

The state equation and output equation can also be indicated in the form of a structural block diagram [15], as shown in the following figure:

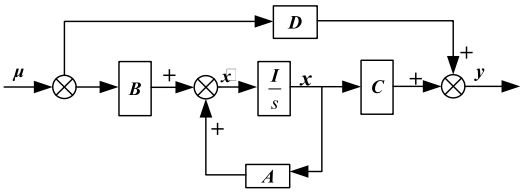

FIGURE 7. Linear system structure diagram.

The Laplace transform of equations (16) and (17) are:

$$s\boldsymbol{X}(s) = \boldsymbol{A}X(s) + \boldsymbol{B}U(s) \tag{18}$$

$$\boldsymbol{Y}(s) = \boldsymbol{C}X(s) + \boldsymbol{D}U(s) \tag{19}$$

Then the forward path transfer matrix of the control system is:

$$\boldsymbol{G}(s) = \boldsymbol{C}(s\boldsymbol{I} - \boldsymbol{A})^{-1}\boldsymbol{B} + \boldsymbol{D} \tag{20}$$

The system open-loop transfer function matrix is:

$$\boldsymbol{H}(s)\boldsymbol{G}(s) = \boldsymbol{H}\left[\boldsymbol{C}(s\boldsymbol{I} - \boldsymbol{A})^{-1}\boldsymbol{B} + \boldsymbol{D}\right] \tag{21}$$

Based on the idea of the state space method, Figure 6 is converted into a system structure diagram:

As the figure illustrates, $\boldsymbol{u} = [u_1\ u_2\ u_3\ u_4]^{\mathrm{T}}$ represents the input vector, which corresponds to $\Delta\varphi_1^*, \Delta\varphi_2^*, \Delta\varphi_3^*, \Delta\varphi_4^*$ in Figure 6; $\boldsymbol{y} = [y_1\ y_2\ y_3\ y_4]^{\mathrm{T}}$ represents the output vector, which corresponds to $\Delta\varphi_1, \Delta\varphi_2, \Delta\varphi_3, \Delta\varphi_4$ in Figure 6; $\boldsymbol{e} = [e_1\ e_2\ e_3\ e_4]^{\mathrm{T}}$ is the control error vector; $\boldsymbol{x} = [x_1\ x_2\ x_3\ x_4\ x_5\ x_6\ x_7\ x_8]^{\mathrm{T}}$ is the state vector, which in turn represents the four eccentric wheels speed and phase; $K_{P1}, K_{P2}, K_{P3}, K_{P4}$ are position loop proportional parameters respectively.

From Figure 8, the state matrix, input matrix, output matrix and feedback matrix of the electric actuator control system are calculated as:

$$\boldsymbol{A} = \begin{bmatrix} -\omega_{cn}\boldsymbol{I}_4 & \boldsymbol{0} \\ \boldsymbol{I}_4 & \boldsymbol{0} \end{bmatrix}_{8\times 8} \tag{22}$$

$$\boldsymbol{B} = \omega_{cn}\begin{bmatrix} K_{P1} & -K_{P1} & 0 & 0 & 0\ 0\ 0\ 0 \\ K_{P2} & K_{P2} & K_{P2} & K_{P2} & 0\ 0\ 0\ 0 \\ K_{P3} & K_{P3} & -K_{P3} & -K_{P3} & 0\ 0\ 0\ 0 \\ 0 & 0 & -K_{P4} & K_{P4} & 0\ 0\ 0\ 0 \end{bmatrix}^T \tag{23}$$

$$\boldsymbol{C} = \begin{bmatrix} 0\ 0\ 0\ 0\ 1 & -1 & 0 & 0 \\ 0\ 0\ 0\ 0\ 1 & 1 & 1 & 1 \\ 0\ 0\ 0\ 0\ 1 & 0 & 0 & -1 \\ 0\ 0\ 0\ 0\ 0 & 0 & -1 & 1 \end{bmatrix} \tag{24}$$

$$\boldsymbol{H} = \begin{bmatrix} 1 & 0 & 0\ 0 \\ 0 & 1/4 & 0\ 0 \\ 0 & 0 & 1\ 0 \\ 0 & 0 & 0\ 1 \end{bmatrix} \tag{25}$$

According to equations (20) and (21), the open-loop transfer function matrix of the electric actuator control system can be calculated as:

$$\boldsymbol{H}(s)\boldsymbol{G}(s) = \frac{\phi_n(s)}{s}\begin{bmatrix} 2K_{P1} & 0 & 0 & 0 \\ 0 & K_{P2} & 0 & 0 \\ K_{P1} & 0 & 2K_{P3} & -K_{P4} \\ 0 & 0 & 0 & 2K_{P4} \end{bmatrix} \tag{26}$$

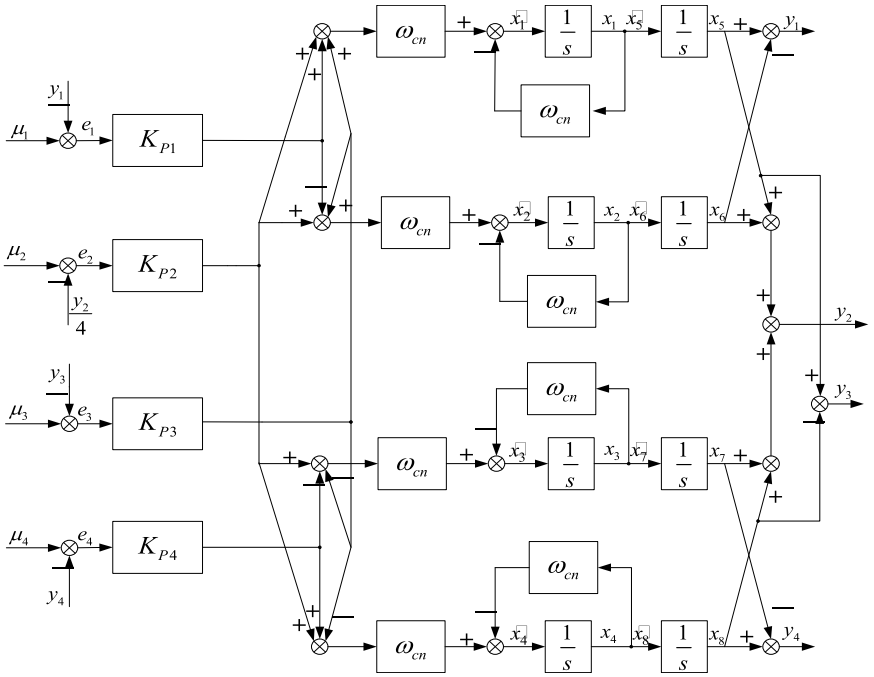

FIGURE 8. Structure diagram of control system of two-dimensional output force vibration elimination electric actuator.

The open-loop transfer function is the basis for analyzing the stability margin of the control system. The stability margin of the single-input single-output linear time-invariant system is usually measured by the phase angle margin and amplitude margin in the frequency domain [16]. The two-dimensional output force vibration damping electric actuator control system proposed in this paper is a multiple-input multiple-output system, and the traditional stability margin calculation method cannot be used to measure the stability boundary of the system. As proposed in the literature [17]–[19], the eigenvalue method of the system return-difference matrix provides a way to solve this problem [17]–[19].

According to the eigenvalue method of the return-difference matrix, the amplitude margin and phase angle margin of the multiple-input multiple-output system are expressed as:

$$\mathrm{GM} = -20\lg(1-\underline{\lambda}) \qquad \mathrm{PM} = 2\arcsin\frac{\underline{\lambda}}{2} \tag{27}$$

Thereinto, $\underline{\lambda}$ is the minimum value of the eigenvalue amplitude of the return-difference matrix of the multiple input multiple output system.

According to equation (26), the return-difference matrix of the electric actuator control system and its eigenvalue amplitude can be obtained as:

$$\boldsymbol{M}(s) = \boldsymbol{H}(s)\boldsymbol{G}(s) + \boldsymbol{I} \tag{28}$$

$$|\lambda_1| = \left|1 + \frac{2K_{P1}\phi_n(s)}{s}\right|_{s=j\omega}$$

$$|\lambda_2| = \left|1 + \frac{K_{P2}\phi_n(s)}{s}\right|_{s=j\omega}$$

$$|\lambda_3| = \left|1 + \frac{2K_{P3}\phi_n(s)}{s}\right|_{s=j\omega}$$

$$|\lambda_4| = \left|1 + \frac{2K_{P4}\phi_n(s)}{s}\right|_{s=j\omega} \tag{29}$$

Taking $K_{\mathrm{P1}} = K_{\mathrm{P2}}/2 = K_{\mathrm{P3}} = K_{\mathrm{P4}} = K_{\mathrm{P}}$, the eigenvalue amplitude can be unified as:

$$|\lambda| = \left|1 + \frac{2K_P\phi_n(s)}{s}\right|_{s=j\omega} \tag{30}$$

Taking the extreme value on the right side of equation (30) in the frequency domain, it can be deduced that the mathematical relationship between the position loop regulator parameter and the mini-mum value of the eigenvalue amplitude is:

$$K_P = \omega_{cn}\frac{(t-1)-\sqrt{2(1-t)}}{2(1-t^2)}, \quad t = \frac{\lambda^2+1}{\lambda^2-1} \tag{31}$$

Since the two-dimensional output force vibration damping electric actuator designed in this paper adopts direct drive structure, and there is no nonlinear interference caused by large gear clearance, so from the perspective of stability and stability margin of control system, the stability margin includes amplitude margin and phase angle margin. Therefore, the index requirements for the control system of vibration elimination actuator are as follows: the range of amplitude margin meets 12 dB $\leq$ GM $\leq$ 22 dB, The range of phase angle margin is 45 ° $\leq$ PM $\leq$ 55 °. From equation (27), the minimum value of the eigenvalue amplitude of the return difference matrix within the corresponding operating frequency range can be calculated to meet the following requirements: 0.77 $\leq$ λ $\leq$ 0.92. If it is brought into

equation (31), the parameter range of the position loop regulator satisfying the stability margin requirement of the control system can be obtained, and the value range is (50,220).

C. OPTIMIZATION OF CONTROLLER PARAMETERS CONSIDERING LOAD DISTURBANCE

The output force of vibration damping electric actuator is realized by the ''opposite throw'' of eccentric wheel load. The eccentric wheel load is different from other constant torque load and belongs to a kind of pulsating load, which will bring load disturbance to the control system so as to cause speed fluctuation and affect the performance of output force. In this section, based on the sensitivity H_∞ control theory [20], the optimal design of the controller parameters is carried out in order to effectively suppress the load disturbance.

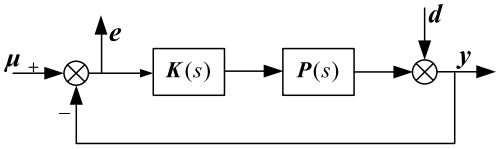

FIGURE 9. Feedback control system.

Figure 9 shows a typical feedback control system. μ is input vector. $\boldsymbol{y}$ is output vector. $\boldsymbol{e}$ is control error vector. $\boldsymbol{d}$ is disturbance vector. $\boldsymbol{K}$(s) and $\boldsymbol{P}$(s) are transfer function matrix of controller and controlled object respectively.

Assuming that $\boldsymbol{S}$(s) represents the transfer function matrix from disturbance $\boldsymbol{d}$ to control error $\boldsymbol{e}$, the H_∞ norm of feedback control system from disturbance to control error is defined as follows:

$$\|\boldsymbol{S}(s)\|_\infty = \sup_{\omega \in R^+} \bar{\sigma}\left\{\boldsymbol{S}(j\omega)\right\} \tag{32}$$

where *sup* is the supremum and $\bar{\sigma}$ is the maximum singular value of the system. It can be expressed as:

$$\bar{\sigma}\left\{\boldsymbol{S}(j\omega)\right\} = \left\{\bar{\lambda}\left[\boldsymbol{S}(j\omega)^H \boldsymbol{S}(j\omega)\right]\right\}^{1/2} \tag{33}$$

H_∞ norm is an extension of the generalized norm and a set of complex function matrices defined in H_∞ space. According to the concept of operator induced norm, the norm of closed-loop control system $\boldsymbol{S}$(s) is defined as:

$$\|\boldsymbol{S}(s)\| = \sup_{\boldsymbol{x} \neq \boldsymbol{0}} \frac{\|\boldsymbol{S}(j\omega)\boldsymbol{x}\|_2}{\|\boldsymbol{x}\|_2} \tag{34}$$

Then, when $\boldsymbol{S}(j\omega) \in H_\infty, \boldsymbol{x} \in \boldsymbol{L}(-\infty, +\infty)$, we have the following conclusions:

$$\|\boldsymbol{S}(s)\| = \sup_{\boldsymbol{x} \neq \boldsymbol{0}} \frac{\|\boldsymbol{S}(j\omega)\boldsymbol{x}\|_2}{\|\boldsymbol{x}\|_2} = \sup_{\omega \in R^+} \bar{\sigma}\left\{\boldsymbol{S}(j\omega)\right\} = \|\boldsymbol{S}(s)\|_\infty \tag{35}$$

It shows that the H_∞ norm of the closed-loop control system is the induced norm of the two norm in H_∞ space. The H_∞ norm of the transfer function matrix $\boldsymbol{S}$(s) represents the maximum gain from disturbance to control error.

According to Figure 9, the closed-loop transfer function from disturbance $\boldsymbol{d}$ to control error $\boldsymbol{e}$ is:

$$\boldsymbol{S}(s) = [\boldsymbol{I} + \boldsymbol{P}(s)\boldsymbol{K}(s)]^{-1} \tag{36}$$

$\boldsymbol{S}$(s) represents the gain from the relative deviation of open-loop characteristics to the relative deviation of closed-loop characteristics. It is also the sensitivity function of the system. The maximum gain of $\boldsymbol{S}$(s) which is the H_∞ norm of $\boldsymbol{S}$(s) can be reduced to a small enough value by designing a reasonable controller $\boldsymbol{K}$(s). Therefore the relative deviation of the closed-loop system can be controlled within the allowable error range in order to minimize the influence of disturbance on the control system.

Combined with formula (28) and (36), the sensitivity function of the electric actuator control system can be calculated as follows:

$$\boldsymbol{S}(s) = \boldsymbol{M}(s)^{-1}\boldsymbol{H}(s) \tag{37}$$

Combined with formula (27), (31) and (33), the H_∞ norm of $\boldsymbol{S}$(s) and the stability margin of the control system under different position loop regulator parameters can be calculated in the simulation software, as shown in the following table:

TABLE 3. Control system performance comparison table under different parameters.

K_P	H_∞ norm	Phase margin	Amplitude margin
50	0.3607	54.77°	21.94 dB
100	0.2812	51.28°	17.42 dB
150	0.1875	48.53°	14.98 dB
200	0.1280	46.25°	13.37dB
250	0.1047	44.30°	12.18 dB

It can be seen from Table 3 that with the increase of the parameter K_P of the position loop regulator, the H_∞ norm of the sensitivity function of the control system decreases gradually, and the anti-interference performance of the system is gradually improved. The amplitude margin decreases from 21.94 dB to 12.18 dB, and the phase margin decreases from 54.77° to 44.3°. The stability margin decreases with the improvement of anti-interference performance. The constant pursuit of the anti-interference ability of the system will inevitably lead to the lack of stability performance. Therefore, considering the stability and anti-interference of the control system, the position loop regulator parameter is 150, which takes into account the anti-interference and stability performance of the control system.

Finally, it is worth mentioning that for the actual control object, in this paper, the four brushless DC motors and the eccentric wheel load driven by them are often constrained by the motor saturation in actual work, thus affecting the normal operation of the actuator. When it is over saturated, it will cause serious heating of the actuator, affect the control accuracy and even burn the motor. Reference [21] provides an effective solution. Based on the dynamic model of the control

system, an output feedback control method is proposed. For the design of the controller, the saturation of the actuator is introduced as a constraint condition, and on this basis, all the control system inputs are within the allowable range, thus avoiding the actuator saturation problem [21]. For the control object proposed in this paper, this method can also be applied to the electric power vibration elimination actuator. The saturation of the actuator is fully considered and the selection range of the controller parameters is further reduced as a constraint condition, so as to ensure that all possible inputs can be controlled within the allowable range.

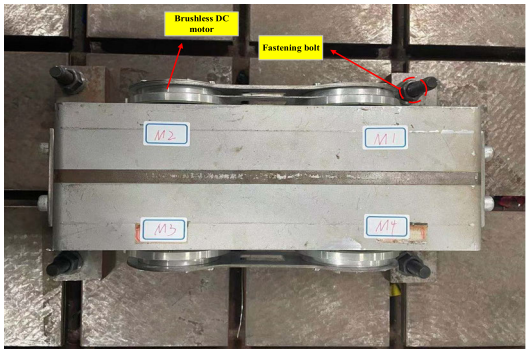

(a) Top view.

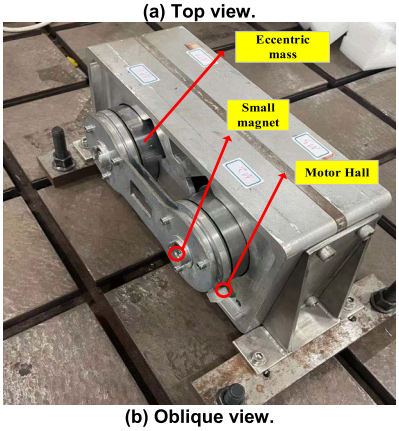

(b) Oblique view.

FIGURE 10. Prototype of two-dimensional output force vibration damping electric actuator.

IV. EXPERIMENTAL VERIFICATION

A. EXPERIMENTAL PLATFORM

In order to verify the effectiveness of the control strategy and the rationality of the optimal design of the controller parameters, the experimental platform of the vibration damping electric actuator system is built, and the output force performance verification experiment is carried out. Figure 10 shows the prototype of two-dimensional output force vibration damping electric actuator. Motors 1# and 4 #, 2 # and 3 # are coaxial motors; 1 # and 2 #, 3# and 4# are the same side motors.The motor on the same side can ''swing'' so as to output the force in any direction on the two-dimensional plane, and the force amplitude of the output force is controlled by controlling the position difference of the coaxial motor. Figure 11 shows the size of the prototype of two-dimensional output force vibration damping electric actuator. The actuator

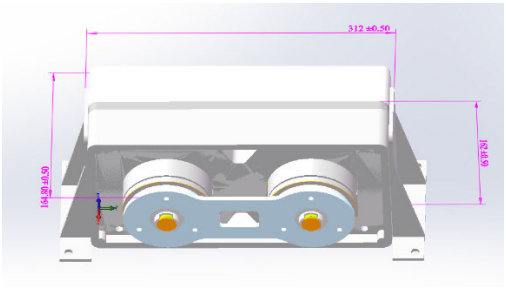

FIGURE 11. Dimensional drawing of the prototype of the two-dimensional output force vibration damping electric actuator.

is 312 mm long, 164.8 mm wide, 162 mm high, with a total weight of 14 kg, which meets the design requirements of small size and light weight of airborne equipment.

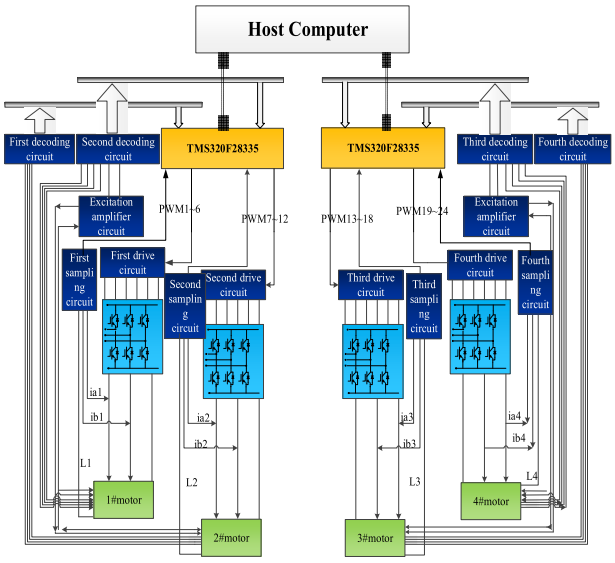

FIGURE 12. Hardware structure block diagram of two-dimensional output force anti vibration electric actuator.

Figure 12 is the system hardware structure block diagram. The controller is divided into the main controller and two sub controllers. The information transmission between the main control and the sub control is carried out through CAN communication. The main controller is responsible for the calculation of the given force and the control of the output force amplitude according to the phase information of the four eccentric wheels transmitted by the sub controller. The sub controller controls the frequency and direction of the output force by controlling two servo motors on the same side of the actuator.

In the experiment, the output force information is collected by the force sensor and sent to the force analyzer, and then the force signal data is fitted in MATLAB. The load speed and position signals are measured by absolute magnetic encoder, and then output by SCI communication module.

Figure 13 is a flow chart of the main program of the control system. After the DSP is powered on, it enters the main program of the system, and the initialization program is performed first. The initialization program mainly includes

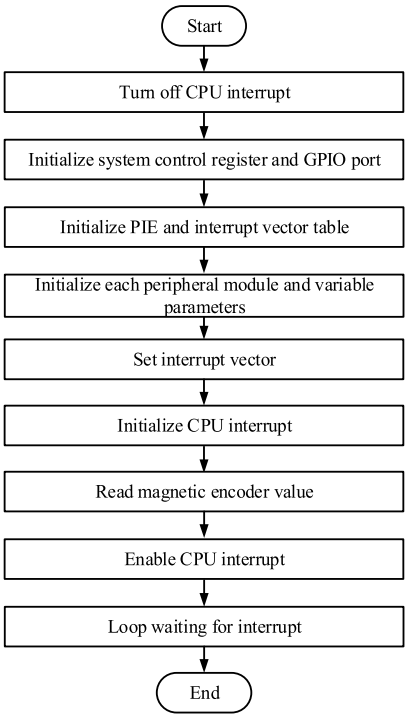

FIGURE 13. The main program flow chart of the two-dimensional output force vibration damping electric actuator.

the initialization of system initialization, GPIO, interrupt vector table, control register, ePWM, AD, eCAP, eCAN, system variables, etc. At the same time, the interrupt vector is set, and the value of the magnetic encoder is read as the initial value of the angular position of the eccentric wheel. Then enter the infinite loop of the main function, waiting for the interrupt request.

The performance index of the two-dimensional output force damping actuator is shown in Table 4.

TABLE 4. Performance index of two dimensional output force damping actuator.

Parameter	Value
Rated operating frequency /Hz	21.5
Working frequency band /Hz	14~30
Maximum output force /N	≥2800
Frequency error	≤0.5%
Steady state error of force amplitude	≤5%
Phase steady state error	≤5%
Change the dynamic settling time of 10% nominal force /s	≤0.5

B. SYNCHRONOUS VERIFICATION TEST OF ACTUATOR SPEED AND POSITION

The control accuracy of the output force of the two-dimensional output force damping actuator depends on the synchronization of the rotation speed and position difference of the eccentric wheel load. When the output force is the vertical maximum force, according to (13), the position difference of 1# eccentric wheel, 2# eccentric wheel on the same side of the actuator, and the coaxial 1# eccentric wheel and 4# eccentric wheel are 0. The actual position difference is shown in Figure 14(a). The load position difference range of two eccentric wheels on the same side is -0.02 rad $\sim$ 0.02rad, and the position difference of coaxial eccentric wheel fluctuates between -0.03 rad$\sim$0.03rad. Since the positions of the two eccentric wheels on the same side and the coaxial shaft are always synchronous, that is to say, the acceleration and deceleration at the same time, the speed difference is small, ranging from -40 rpm to 40rpm, as shown in Figure 15(a). When the output force is the vertical minimum force, theoretically, the position difference of two eccentric wheels on the same side of the actuator is 0, and the position difference of coaxial eccentric wheel is 1rad. The actual position difference is shown in Figure 14(b). The load position difference range of two eccentric wheels on the same side is -0.02 rad $\sim$ 0.02rad, and the position difference of coaxial eccentric wheel fluctuates between 3.08rad $\sim$ 3.20rad, and the fluctuation range is larger than that on the same side. This is mainly because for eccentric load, when the eccentric wheel moves from the lowest point of mechanical position to the highest point, the load torque is resistance torque for the motor, and the motor decelerates; when the eccentric wheel changes from the lowest point to the highest point, the load torque changes into dynamic torque and the motor accelerates. When the position difference is πrad, one eccentric wheel accelerates while the other decelerates, so the speed difference and position difference pulsation are large. As shown in Figure 15(b), the load speed difference of two eccentric wheels on the same axis is $\pm$60 rpm. When the actuator output force is the horizontal maximum force, the position difference and speed difference waveform are shown in Figure 14(c) and Figure 15(c). The load position difference range of two eccentric wheels on the same side is 3.10rad $\sim$ 3.18rad, and the speed difference is $\pm$60rpm; the coaxial load position difference is -0.03 rad$\sim$0.03rad, and the speed difference is $\pm$40rpm. Figure 14(d) and 15(d) show the load position difference and speed difference waveform when the actuator output force is the minimum horizontal force. The load position difference range of the two eccentric wheels on the same side and the coaxial is 3.10rad$\sim$3.18rad, and the speed difference is $\pm$ 60rpm.

C. STEADY STATE VERIFICATION TEST OF ACTUATOR OUTPUT FORCE

In order to meet the needs of helicopter vibration reduction, the maximum output force of the two-dimensional output force vibration damping actuator must be greater than or equal to 2800N, and when the power output of the actuator is 0, it should not produce excessive impact. Figure 16 and 17 respectively show the minimum output force and maximum output force waveforms at the rated

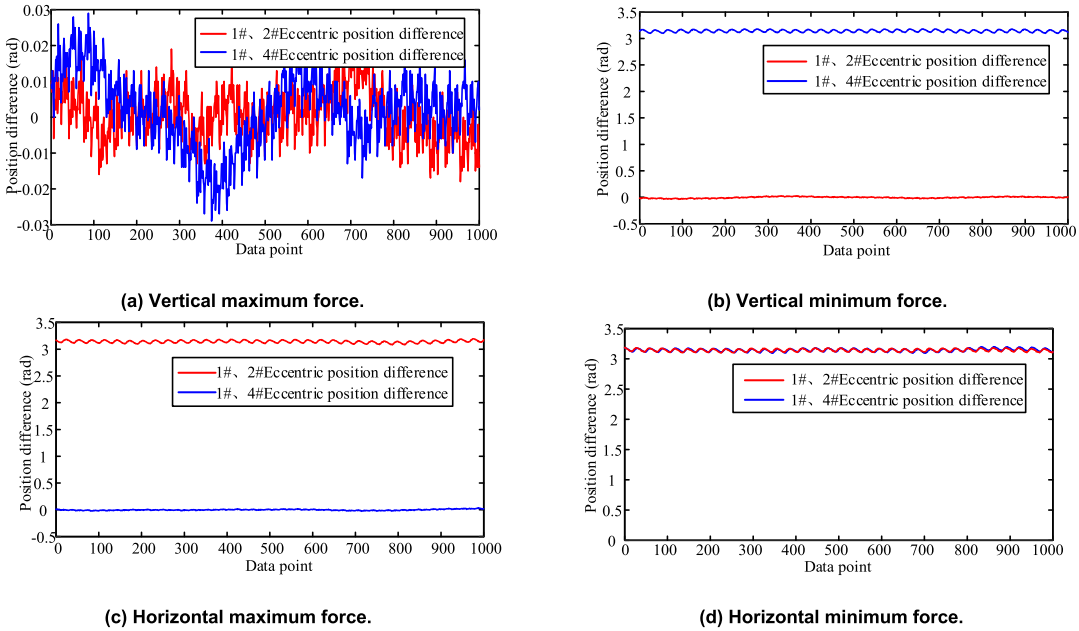

(a) Vertical maximum force.

(b) Vertical minimum force.

(c) Horizontal maximum force.

(d) Horizontal minimum force.

FIGURE 14. Position difference waveform of eccentric wheel of two-dimensional output force damping actuator.

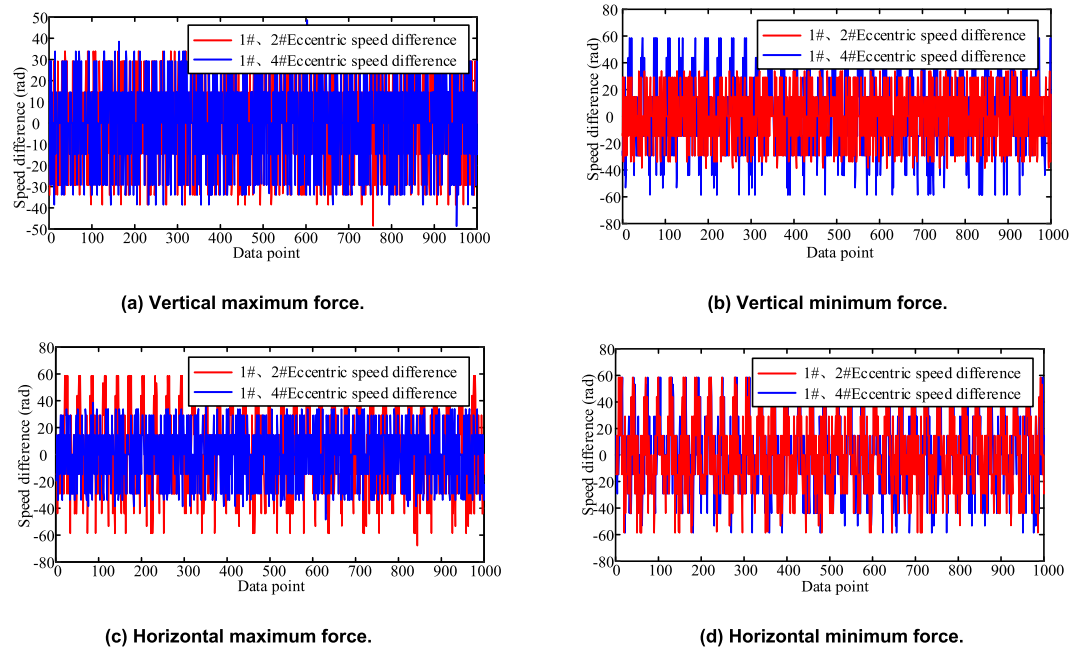

(a) Vertical maximum force.

(b) Vertical minimum force.

(c) Horizontal maximum force.

(d) Horizontal minimum force.

FIGURE 15. Two-dimensional output force damping actuator eccentric wheel speed difference waveform.

operating frequency of the actuator. Figure 18 shows the Fourier analysis waveform of the maximum output force of the actuator at rated operating frequency.

It can be seen from Figure 16 that the minimum output force of the two-dimensional output force damping actuator fluctuates between ±150N without excessive impact. It can be seen from Figure 17 that when the operating frequency of the actuator is set as 21.5Hz, the maximum output force is 3396N, which meets the index requirement of 2800N or more. At the same time, it can be seen from Figure 18 that the FFT analysis of the maximum output force shows that the actual work of the actuator is 21.5 Hz, which is equal to the given operating frequency and has no frequency error, indicating that the system has good steady-state performance.

D. DYNAMIC VERIFICATION TEST OF ACTUATOR OUTPUT FORCE

In the flight process of helicopter, the frequency, amplitude, direction and phase of the vibration force generated by the rotor and tail rotor are not invariable. Therefore, not only the excellent steady-state performance of the actuator is required, but also the high dynamic performance is required. In this two-dimensional output force damping actuator, the dynamic settling time of 10% nominal force change is required to

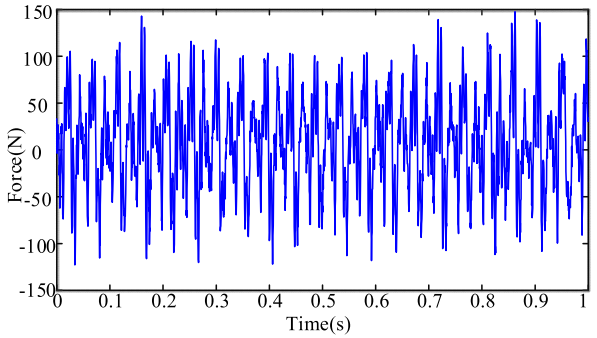

FIGURE 16. Minimum output force waveform of two-dimensional output force damping actuator.

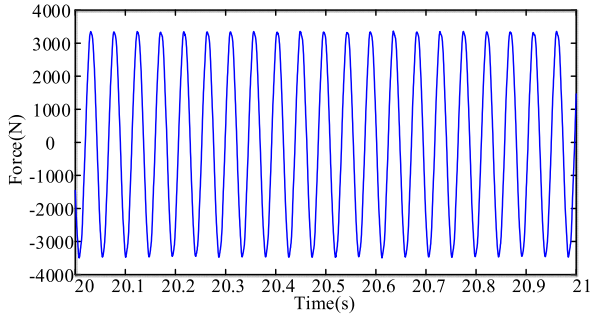

FIGURE 17. Maximum output force waveform of two-dimensional output force damping actuator.

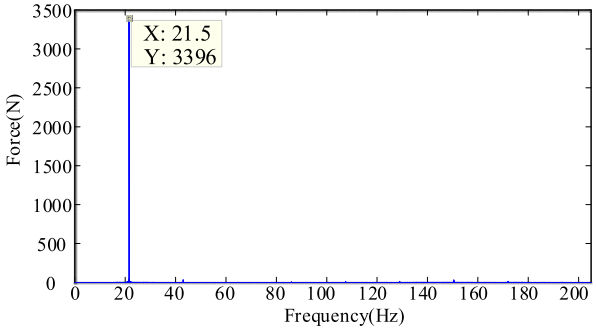

FIGURE 18. FFT analysis of maximum output force of two-dimensional output force damping actuator.

be less than 0.5s, and the commands of frequency change 1Hz, amplitude change 10%, direction change 15° and phase change 60° are sent to the actuator in turn. The output force waveform is shown in Figure 19–22.

Figure 19 shows that the dynamic settling time of the output force frequency of the two-dimensional output force damping actuator from 20Hz to 21Hz is 0.47s. It can be seen from Figure 20 that the actuator output force amplitude is 2728N at 0.32s, when the time is 0.57s, the actuator output force amplitude changes from 2728N to 3000N, and the dynamic adjustment time is 0.25s.With the actuator output force vertically downward as zero angle, the direction of output force is adjusted by adjusting the position difference between the two eccentric wheels on the same side of the

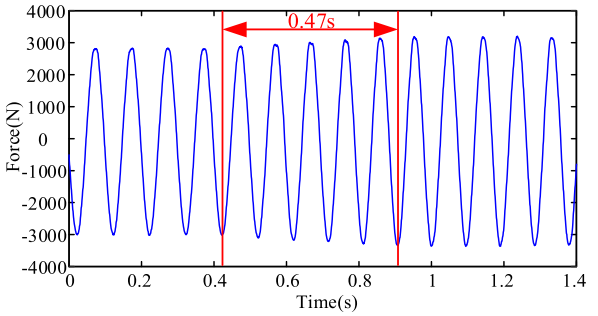

FIGURE 19. 1Hz waveform of output force frequency variation of two-dimensional output force damping actuator.

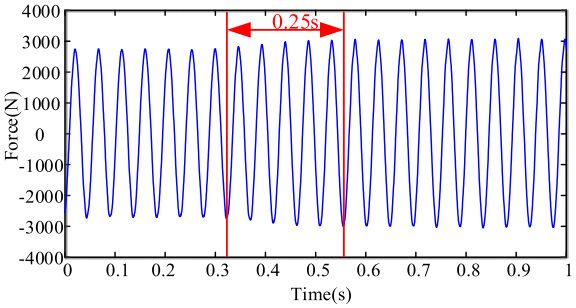

FIGURE 20. Waveform of 10% change of output force amplitude of two-dimensional output force damping actuator.

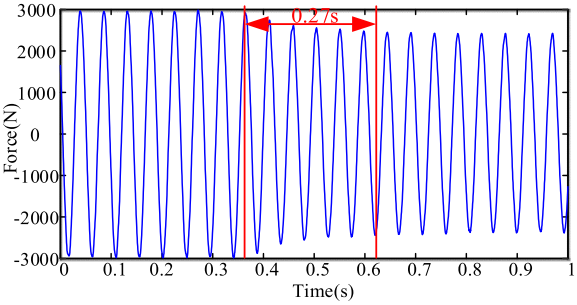

(a) Vertical output force.

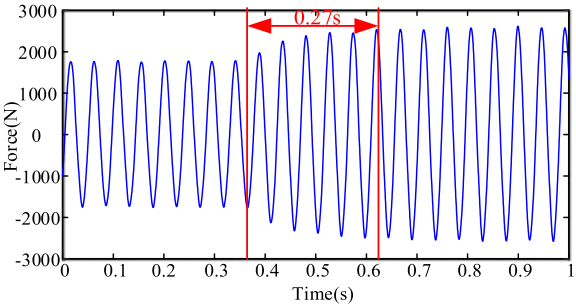

(b) Horizontal output force.

FIGURE 21. Waveform of two-dimensional output force damping actuator with 15 degree change of output force direction.

actuator to meet the demand of multi-directional vibration reduction. It can be seen from Figure 21 that the settling time is 0.27s when the output force direction of the actuator changes from 30° to 45°. It can be seen from Figure 22 that the settling time for the phase change of actuator output force

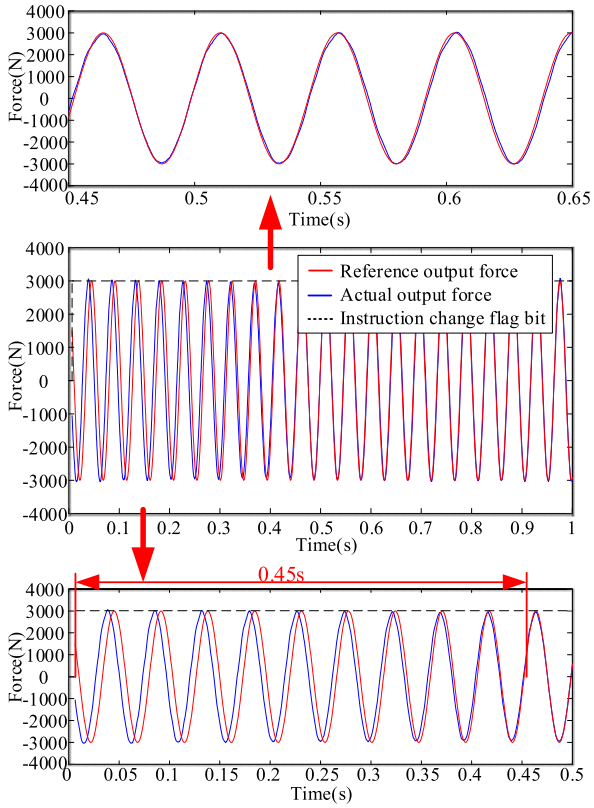

FIGURE 22. The output force phase of the two-dimensional output force damping actuator changes to 60 degree waveform.

to 60° is 0.45s, and there is almost no steady-state error. According to Figure 19–22, the actual output force of the actuator can quickly keep up with the given value, meet the requirements of the index, and there is almost no steady-state error after stabilization. The system has good dynamic and steady-state performance, which verifies the effectiveness of cross coupling control strategy and the rationality of synchronous ring parameter design.

V. CONCLUSION

Aiming at the problem that linear actuators have large gear gap nonlinearity and can only output unidirectional force, a two-dimensional output force vibration reduction actuator system is proposed, and the following conclusions are obtained:

1)Two-dimensional output force damping actuator system uses four motors to directly drive their eccentric wheel load structure. Firstly, the mathematical expression of one-side output force of damping actuator is derived, and the time-space coupling method of relative coordinate system is proposed to model the two-dimensional output force of actuator. So that the actuator can output force in the direction of 360°.

2)A cross coupling control strategy based on spatiotemporal coupling method in rotating coordinate system is proposed. By controlling the direction of output force first and then the amplitude, the decoupling of the direction and amplitude of the two-dimensional output force is realized. The output force direction is controlled by controlling the position difference of two eccentric wheels on the same side of the actuator, and the output force amplitude is controlled by controlling the position difference of the coaxial eccentric wheel. The frequency and phase of the output force can be changed by changing the speed of the eccentric wheel and the current angle position. Finally, the frequency, phase, amplitude and direction of the output force of the actuator can be controlled.

3)For the cross coupling control strategy, considering the influence of system coupling, the parameters of synchronization loop are designed by the eigenvalue method of return difference matrix based on stability margin, and the parameter range meeting the requirements of stability margin is obtained. At the same time, both anti-interference and torque ripple suppression are taken into account. According to the sensitivity H_∞ control theory, the design method is simple and effective.

4)The two-dimensional output force vibration damping electric actuator has the advantages of small size, light weight, smart installation and convenient maintenance. At the same time, it can output the power in any direction on the two-dimensional plane, which can effectively offset the vibration force on the helicopter and improve the fuselage Vibration environment; but at present, the design method of this paper has not dealt with the saturation problem of the actuator. When the motor is saturated, it will inevitably affect the control accuracy of the output force, and it is necessary to use the motor saturation as a constraint condition in the following research. Optimize the parameter design of the controller.

REFERENCES

[1] J. D. Leatherwood, S. A. Clevenson, and D. D. Hollenbaugh, "Evaluation of ride quality prediction methods for helicopter interior noise and vibration environments," NASA, Washington, DC, USA, Tech. Rep., 1984.
[2] C. E. Hammond, D. D. Hollenbaugh, S. A. Clevenson, and J. D. Leatherwood, "An evaluation of helicopter noise and vibration ride qualities criteria," NASA, Washington, DC, USA, Tech. Rep. Memorandum, 1982.
[3] S. Lee, K. Hirata, F. Kitayama, and E. Hong, "Active vibration damping of linear oscillatory actuator using DC motor," in *Proc. 42nd Annu. Conf. IEEE Ind. Electron. Soc. (IECON)*, Florence, Italy, Oct. 2016, pp. 1762–1766, doi: 10.1109/IECON.2016.7793236.
[4] M. Mihai, A. Arcire, and R. Olaru, "Vibration mini actuator with magnetically suspended inertial mass," in *Proc. Int. Conf. Expo. Electr. Power Eng. (EPE)*, Iasi, Romania, 2016, pp. 083–086, doi: 10.1109/ICEPE.2016.7781308.
[5] G. C. Han, H. Li, and Z. Q. Wang, "Research on marine electric vibration elimination actuator," *J. Harbin Eng. Univ.*, vol. 2005, no. 1, pp. 39–43, 2005.
[6] K. D. Garnjost and G. J. Rey, "Modular vibratory force generator, and method of operating same," U.S. Paten 5 903 077, May 11, 1999.
[7] X. Q. Lu, D. J. Wang, and A. D. Zhang, "Experimental research on active vibration control based on mechanical actuator," *Noise Vib. Control*, vol. 4, pp. 1–2 and 5, 2008.
[8] Z. Y. Hao, X. Li, X. Cao, Y. Gan, and Q. Yu, "Position difference cross coupling control strategy for electric power vibration damping actuator," *Acta Aeronautica Sinica*, vol. 1104, pp. 1–12, 2020.
[9] C. Qi-You, D. Jing-Hui, H. Jian-Ping, L. Ai-Min, and L. Ke, "Optimization selection approach for distribution of actuators in active vibration control of helicopter," in *Proc. 34th Chin. Control Conf. (CCC)*, Hangzhou, China, 2015, pp. 3248–3251, doi: 10.1109/ChiCC.2015.7260140.

[10] D. Dong-Pyo, H. Ha-Young, L. Moo-Yeon, J. Yang-Keun, V. Duc-Thuan, and L. Dong-Yeon, "New electro-magnetic actuator for active vibration isolators," *Int. J. Precis. Eng. Manuf.*, vol. 16, no. 1, pp. 209–212, 2015.
[11] P. Vartholomeos, K. Vlachos, and E. Papadopoulos, "Analysis and motion control of a centrifugal-force microrobotic platform," *IEEE Trans. Automat. Sci. Eng.*, vol. 10, no. 3, pp. 545–553, Jul. 2013.
[12] R. Guo, "Three-loop positioning servo system of ultra-precision machine tool using adaptive reference modelling," in *Proc. Int. Conf. Mech. Sci., Electr. Eng. Comput. (MEC)*, Shengyang, China, 2013, pp. 330–334, doi: 10.1109/MEC.2013.6885092.
[13] Z. M. Han, *Research on Control Strategy of PMSM Direct Drive Position Servo System*. Nanjing, China: Nanjing Univ. of Aeronautics and Astronautics, 2017, pp. 11–20.
[14] V. Ignatenko, A. Yudintsev, and D. Lyapunov, "Application of state-space method for control system analysis," in *Proc. Int. Siberian Conf. Control Commun. (SIBCON)*, Tomsk, Russia, 2019, pp. 1–5, doi: 10.1109/SIBCON.2019.8729658.
[15] D. Z. Zheng, *Linear System Theory*. Beijing, China: Tsinghua Univ. Press, 2002.
[16] F. Li, Y. Hong, Z. Xiong, and J. Wang, "Stability margin analysis of multivariable aircraft control system under single loop perturbation," in *Proc. 32nd Chin. Control Conf.*, Xi'an, China, 2013, pp. 1448–1452.
[17] V. Mukhopadhyay, "Application of matrix singular value properties for evaluating gain and phase margins of multiloop systems," in *Proc. AIAA Guid. Navigat. Control Conf.*, 1982, pp. 9–11.
[18] Q. G. Wang, Y. He, Z. Ye, C. Lin, and C. C. Hang, "On loop phase margins of multivariable control systems," *J. Process Control*, vol. 18, no. 18, pp. 202–211, 2008.
[19] X. D. Li and X. Y. Gou, "Degenerate algorithm for finding stability margin from singular value of hysteresis matrix," *Control Theory Appl.*, vol. 33, no. 4, pp. 460–465, 2016.
[20] L. Yu, C. Che, J. Guo, and H. Wang, "The design of H_∞ mixed sensitivity controller for fin/tank roll stabilizer," in *Proc. 35th Chin. Control Conf. (CCC)*, Chengdu, China, 2016, pp. 2929–2933, doi: 10.1109/ChiCC.2016.755380.
[21] T. Yang, N. Sun, H. Chen, and Y. Fang, "Observer-based nonlinear control for tower cranes suffering from uncertain friction and actuator constraints with experimental verification," *IEEE Trans. Ind. Electron.*, early access, May 12, 2020, doi: 10.1109/TIE.2020.2992972.

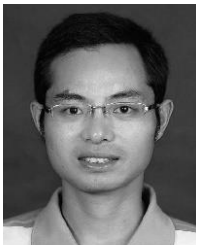

ZHENYANG HAO received the bachelor's degree in electrical engineering from Nanjing Normal University, in 2004, and the master's and doctor's degrees in power electronics and motion drive from the Nanjing University of Aeronautics and Astronautics, in 2010.

He has been an Associate Professor with the Department of Electrical Engineering, Nanjing University of Aeronautics and Astronautics, since 2013. His research interests include new energy power electronic conversion technology, aviation power supply and power actuator technology, electric vehicle motor design, and driving technology.

TAO WANG received the degree in electrical engineering and automation from Anhui University, in 2019. He is currently pursuing the master's degree in electrical engineering with the Nanjing University of Aeronautics and Astronautics, China. His research interests include active vibration control and motor control.

XIN CAO (Member, IEEE) received the B.Eng., M.Sc., and Ph.D. degrees in electrical engineering from the Nanjing University of Aeronautics and Astronautics, Nanjing, China, in 2003, 2006, and 2010, respectively, all in electrical engineering. Since 2011, he has been with the Nanjing University of Aeronautics and Astronautics. From June 2011 to September 2012, he was a Research Associate with the Department of Aeronautical and Automotive Engineering, Loughborough University, Loughborough, U.K. His current research interests include distributed generation and renewable energy, electric vehicles, switched reluctance motors, and magnetically levitated bearingless motors.

XUE LI received the degree in electrical engineering from the Nanjing University of Aeronautics and Astronautics, China, in 2018, where she is currently pursuing the master's degree in electrical engineering.

Her current research interest includes multi-motor coordinated control.

QIYAO ZHANG (Student Member, IEEE) received the degree in electrical engineering and automation from the Nanjing University of Aeronautics and Astronautics, China, in 2020, where she is currently pursuing the master's degree in electrical engineering. Her research interest includes motor control.